



# Design and synthesis of nanoscale titanium-porphyrin coordination nanomaterials for photodynamic-sonodynamic synergistic therapy of tumor cells

Wei Wang<sup>1†</sup>, Wenquan Huang<sup>2†</sup> , Liu Huang<sup>3†</sup>, Yan Li<sup>1</sup>, Shuzhang Xiao<sup>1,4\*</sup> , Haichuang Lan<sup>1</sup>, Peng Geng<sup>1,2,4\*</sup> 

<sup>1</sup>Key Laboratory of Inorganic Nonmetallic Crystalline and Energy Conversion Materials, College of Materials and Chemical Engineering, China Three Gorges University, Yichang 443002, Hubei, China

<sup>2</sup>College of Medicine and Health Science, China Three Gorges University, Yichang 443002, Hubei, China

<sup>3</sup>College of Basic Medical Science, China Three Gorges University, Yichang 443002, Hubei, China

<sup>4</sup>Hubei Three Gorges Laboratory, Yichang 443007, Hubei, China

<sup>†</sup>These authors share the first authorship.

\***Correspondence:** Shuzhang Xiao, [shuzhangxiao@ctgu.edu.cn](mailto:shuzhangxiao@ctgu.edu.cn); Peng Geng, [gengpeng@ctgu.edu.cn](mailto:gengpeng@ctgu.edu.cn). Key Laboratory of Inorganic Nonmetallic Crystalline and Energy Conversion Materials, College of Materials and Chemical Engineering, China Three Gorges University, Yichang 443002, Hubei, China

**Academic Editor:** Laichang Zhang, Edith Cowan University's School of Engineering, Australia

**Received:** September 28, 2024 **Accepted:** April 10, 2025 **Published:** April 24, 2025

**Cite this article:** Wang W, Huang W, Huang L, Li Y, Xiao S, Lan H, et al. Design and synthesis of nanoscale titanium-porphyrin coordination nanomaterials for photodynamic-sonodynamic synergistic therapy of tumor cells. *Explor BioMat-X*. 2025;2:101337. <https://doi.org/10.37349/ebmx.2025.101337>

## Abstract

**Aim:** Multifunctional nanomaterials with photodynamic-sonodynamic therapy (PSDT) potential offer significant advantages in cancer treatment. However, designing and preparing single-component “two-in-one” multifunctional nanomaterials remains challenging. Hematoporphyrin monomethyl ether (HMME), a second-generation porphyrin-related sonosensitizer, is a porphyrin derivative with two asymmetric carboxyl groups. Notably, the carboxyl groups in HMME can coordinate with metal ions to construct metal-organic coordination nanomaterials (MCPs). Titanium (Ti), a biocompatible metal element, is commonly used in medical devices such as implantable metal alloys. Therefore, this study reported the synthesis of “two-in-one” type Ti-HMME coordination nanomaterials (TiCPs) as efficient nanoscale photo/sonosensitizers.

**Methods:** Under a nitrogen atmosphere, TiCPs were synthesized via self-assembly between HMME and Ti<sup>4+</sup> ions.

**Results:** The average particle size of TiCPs was approximately 70 nm. Additionally, TiCPs contained the photo/sonosensitizer HMME, which could convert O<sub>2</sub> into cytotoxic reactive oxygen species (ROS) under light and ultrasound (US) excitation. The generation of ROS could be detected using 1,3-diphenylisobenzofuran (DPBF). When the mixed solution (TiCPs + DPBF) was irradiated with light, the DPBF peak rapidly decreased with increasing irradiation time, indicating the production of ROS by TiCPs under light. Similarly, the absorbance of TiCPs + DPBF significantly decreased with increasing US time, demonstrating the sonodynamic effect of TiCPs + US. After 10 min of light or US excitation, 49.4% (Light)

© The Author(s) 2025. This is an Open Access article licensed under a Creative Commons Attribution 4.0 International License (<https://creativecommons.org/licenses/by/4.0/>), which permits unrestricted use, sharing, adaptation, distribution and reproduction in any medium or format, for any purpose, even commercially, as long as you give appropriate credit to the original author(s) and the source, provide a link to the Creative Commons license, and indicate if changes were made.



and 38.1% (US) of DPBF were oxidized by ROS generated by TiCPs, showcasing excellent photodynamic/sonodynamic effects. In vitro cell experiments further demonstrated that TiCPs had excellent biocompatibility, could be effectively internalized by cells, and significantly reduced cell viability under light and US excitation, effectively killing tumor cells.

**Conclusions:** This study not only demonstrated TiCPs as “two-in-one” type multifunctional nanomaterials for PSDT but also provided insights into designing other photo/sonosensitizer molecules with similar HMME structures for tumor theranostics.

## Keywords

Metal-organic coordination nanomaterials, two-in-one, hematoporphyrin monomethyl ether, photodynamic therapy, sonodynamic therapy

---

## Introduction

Malignant tumors present a significant threat to human health, and current cancer treatments continue to face substantial challenges in terms of both effectiveness and limitations [1, 2]. In addition to conventional methods like surgery, chemotherapy, and radiotherapy, there is a pressing need for the development of innovative, minimally invasive therapies for more effective tumor treatment, such as photodynamic therapy (PDT) [3, 4], photothermal therapy (PTT) [5, 6], and sonodynamic therapy (SDT) [7, 8]. Light-based therapies like PDT and PTT typically use near-infrared light or lasers within a safe intensity range, minimizing skin tissue damage and offering high safety [9, 10]. However, the treatment of deep-seated tumors remains challenging due to the rapid attenuation of light as it passes through skin tissues. To overcome the limitation of light penetration, SDT, which utilizes ultrasound (US) as an excitation source, has gained considerable attention [11, 12]. As a mechanical wave, US is commonly used in clinical imaging, offering well-established safety, low cost, and a penetration depth in soft tissues exceeding 10 cm [13]. This makes US-triggered SDT therapy ideal for achieving both excellent biocompatibility and deeper tissue penetration [14, 15]. However, the efficiency of reactive oxygen species (ROS) generation with SDT-excited sonosensitizers is generally lower than that of PDT-excited photosensitizers. To enhance treatment efficiency, combining PDT with SDT (PSDT) can leverage their complementary strengths and achieve synergistic therapeutic effects [16, 17]. The success of PSDT synergistic therapy depends on the development of multifunctional nanomaterials with effective photo/sonosensitizing capabilities.

So far, researchers have combined photo/sonosensitizers for PSDT through various methods, including carrier encapsulation, chemical conjugation, and physical adsorption [18, 19]. For instance, by encapsulating the photo/sonosensitizers hematoporphyrin monomethyl ether (HMME) and rose bengal within a porous SiO<sub>2</sub> nanocarrier, effective PSDT treatment outcomes have been achieved [19]. However, the loading efficiency of organic small molecule photo/sonosensitizers is often suboptimal, and their release tends to be spontaneous. Moreover, most composite materials comprise multiple components, making their synthesis process rather complex. Therefore, designing and synthesizing single-component, “all-in-one” multifunctional nanomaterials holds significant research value [20–22].

Recently, metal-organic coordination nanomaterials (MCPs), composed of metal ions and organic ligands, have received widespread attention across various fields [23, 24]. These MCPs offer advantages such as high porosity, good hydrophilicity, biodegradability, and ease of functionalization. In biomedical applications, photo/sonosensitizing small molecules can serve as organic ligands that coordinate with metal ions to form functional MCPs, addressing challenges like poor water solubility, low chemical stability, and suboptimal tumor targeting of organic photo/sonosensitizers [25, 26]. For example, MCPs containing tetra (4-carboxyphenyl) porphyrin (TCPP), known for their PDT effects, have shown promising potential in tumor treatments, including Zr-TCPP MCPs [27, 28], Cu-TCPP MCPs [29, 30], Mn-TCPP MCPs [31], and Gd-TCPP MCPs [32]. However, in the context of tumor SDT, reports on MCP-based sonosensitizers remain scarce, particularly those exhibiting combined PSDT therapeutic capabilities.

As a novel second-generation porphyrin-based sonosensitizer, HMME is a derivative of hematoporphyrin that contains two asymmetric carboxyl groups [33, 34]. Notably, the carboxyl groups in HMME can coordinate with metal ions, serving as bridging groups to construct MCPs. Titanium (Ti), a biocompatible metal element, is frequently used in medical devices, such as implantable metal alloys [35, 36]. In this study, we developed a Ti-HMME coordination nanomaterial (TiCPs) through the covalent coordination self-assembly of titanium ions and HMME molecules. The synthesized TiCPs demonstrated excellent biocompatibility in cytotoxicity experiments and exhibited efficient PDT and SDT effects under light and US stimulation. Therefore, this study not only demonstrates the potential of TiCPs as a “two-in-one” nanomedicine for PSDT therapy but also offers valuable insights for designing other molecules with structures similar to HMME for biomedical applications.

## Materials and methods

### Materials

HMME (analytical grade, supplied by Shanghai Macklin Biochemical Co., Ltd.); titanium tetrachloride (TiCl<sub>4</sub>, analytical grade, from Shanghai Macklin Biochemical Co., Ltd.); 1,3-Diphenylisobenzofuran (DPBF, spectrally pure, obtained from Shanghai Aladdin Biochemical Technology Co., Ltd.), among others. Mice colorectal cancer (CT26) cells and human umbilical vein endothelial cells (HUVEC) were purchased from the Chinese Academy of Sciences. STR species contamination identification of CT26: (1) STR profiling of the cell's DNA confirmed that it belongs to mouse cells; (2) the STR data of this cell matches 100% with that of CT26.WT cells in the EXPASy database; (3) no evidence of human cell contamination was detected in this cell.

### Synthesis procedure

Dissolve 2 mg of HMME in a mixture of triethylamine (0.5 mL) and DMF (8 mL), stirring under a nitrogen atmosphere for 30 min. Transfer the resulting mixture into a 25 mL reaction vessel and add TiCl<sub>4</sub> solution (20 μL) under nitrogen. Allow the reaction to proceed at 110°C for 4 h. Upon completion, cool the reaction mixture to 25°C. The product is then collected by centrifugation and washed three times each with DMF and anhydrous ethanol to yield the target compound.

### Characterization

Morphology and composition of samples were characterized by using JSM-7500F Scanning Electron Microscope (SEM, JEOL, Japan, operating at 10 kV) and AXIS Supra X-ray Photoelectron Spectrometer (XPS, Shimadzu, Japan). Zeta potential was carried out on a nano particle size and ZETA potential analyzer (NANOTRAC WAVE II, USA). The photo-absorption and fluorescence were recorded using a UV-2600 Spectrophotometer (Shimadzu, Japan) and a fluorescence spectrometer (F4600), respectively.

### ROS generation assay

First, prepare the ROS probe by dissolving DPBF in DMF. Next, add the DPBF solution (20 μL), to a TiCPs solution (4 mL, 50 μg·mL<sup>-1</sup> in DMF) to form a uniform mixture. Illuminate this mixture with a light source (630 nm, 100 mW·cm<sup>-2</sup>) to assess the ROS generation efficiency of TiCPs under photodynamic conditions, or expose it to US (2.0 W·cm<sup>-2</sup>) to evaluate sonodynamic ROS production. Bubble air through the mixture for 30 s every 2 min, and monitor changes in the absorption spectrum using a UV-vis spectrophotometer. To compare the ROS generation efficiency under different stimuli, record the absorption spectra for DPBF alone and TiCPs with light/US exposure under identical conditions.

### Cell cytotoxicity assay

Mice colorectal cancer (CT26) cells and human umbilical vein endothelial cells (HUVEC) were cultured in RPMI-1640 medium with 10% FBS and 1% penicillin-streptomycin under standard conditions. The cell lines were confirmed to be free from mycoplasma and other contaminants. CT26 cells were plated in 96-well plates at a density of  $1 \times 10^4$  cells per well and incubated for 24 and 48 h. TiCPs were then added at

concentrations of 0–400  $\mu\text{g}\cdot\text{mL}^{-1}$ . After incubation, cells were washed twice with PBS and treated with fresh medium containing MTT for 2 h. The supernatant was discarded, and 100  $\mu\text{L}$  of DMSO was added to dissolve the formazan crystals. Absorbance was measured at 490 nm using a microplate reader, with five independent replicates.

### Endocytosis and ROS generation within cells

To examine the endocytosis of TiCPs, CT26 cells were plated in 12-well plates at a density of  $2 \times 10^5$  cells per well and cultured for 12 h. TiCPs at a concentration of 200  $\mu\text{g}\cdot\text{mL}^{-1}$  were then added to each well. After incubation for 0.5, 1, 3, and 5 h, the cells were washed with PBS and imaged using a digital microscope. To investigate the intracellular ROS generated by TiCPs, the cells were treated with TiCPs at 200  $\mu\text{g}\cdot\text{mL}^{-1}$  for 4 h, then washed twice with PBS. A fresh medium containing 20  $\mu\text{M}$  2',7'-dichlorofluorescein diacetate (DCFH-DA) was added for co-culture for an additional 30 min. The cells were then exposed to 630 nm light at 100  $\text{mW}\cdot\text{cm}^{-2}$  for 5 min (TiCPs + Light group), US at 2.0  $\text{W}\cdot\text{cm}^{-2}$  for 5 min (TiCPs + US group), or both (TiCPs + Light + US group). For comparison, cells without TiCPs were also subjected to light (Light group) or US (US group) under identical conditions. After treatment, the cells were stained with DAPI for 20 min before imaging.

### Photodynamic/sonodynamic therapy in cells

Incubate CT26 cells with TiCPs (200  $\mu\text{g}\cdot\text{mL}^{-1}$ ) for 5 h. Then, irradiate the cells using light (630 nm, 100  $\text{mW}\cdot\text{cm}^{-2}$ ) and/or US (2.0  $\text{W}\cdot\text{cm}^{-2}$ ) for different durations. Evaluate cell viability using the MTT assay, or perform co-staining with Calcein-AM/PI to capture fluorescence images, allowing assessment of the therapeutic effects across different treatment groups.

### Statistical analysis

The data are presented as the mean  $\pm$  standard deviation (SD), and statistical analysis was performed using Student's two-tailed *t*-test. \**p* < 0.05 (significant), \*\**p* < 0.01 (moderately significant), and \*\*\**p* < 0.001 (highly significant).

## Results

### Morphology and element valence analysis of TiCPs

Under a nitrogen atmosphere, TiCPs were synthesized via self-assembly between HMME and  $\text{Ti}^{4+}$  ions (Figure 1a). The morphology and size of TiCPs were subsequently investigated using SEM. The SEM images revealed that TiCPs exhibited a quasi-spherical shape with an average size of approximately 70 nm (Figure 1b). The surface elemental states of the sample were determined using XPS. The overall XPS spectrum of TiCPs (Figure 1c) shows the corresponding signals of Ti, C, N, and O elements, where Ti signals are from  $\text{Ti}^{4+}$  ions [8, 35], while C, N, and O signals are from HMME ligands. A distinct Ti peak observed at 455 eV confirms the successful incorporation of Ti into HMME. The high-resolution Ti 2p spectrum (Figure 1d) displays two peaks at binding energies of 464.5 eV and 458.6 eV, corresponding to the Ti 2p<sub>1/2</sub> and Ti 2p<sub>3/2</sub> orbitals, respectively, indicating that Ti in the sample is in a +4 oxidation state. The peak at approximately 460 eV suggests that  $\text{Ti}^{4+}$  is coordinated with the oxygen atoms on the carboxyl groups of HMME. The C 1s spectrum (Figure S1) was deconvoluted into three peaks. The main peak at 284.7 eV corresponds to C=C bonds in TiCPs. The additional peaks at 286.2 eV and 289.2 eV are attributed to C–O (C–N) bonds and C=N bonds in TiCPs, respectively.

To gain further insight into the interaction between  $\text{Ti}^{4+}$  ions and HMME within TiCPs, UV-vis spectroscopy, FTIR spectroscopy, and FL spectroscopy were conducted. The UV-vis spectrum of HMME showed a major peak around 399 nm (Soret band) along with four smaller peaks in the 470–630 nm range (Q-bands). In comparison, TiCPs retained distinct Soret and Q-bands (Figure 2a). Notably, the presence of four peaks in the Q-band of TiCPs, instead of two or three, indicates that  $\text{Ti}^{4+}$  ions coordinate specifically with the carboxyl groups of HMME rather than the central porphyrin ring [21, 25]. The FTIR spectrum of TiCPs revealed the disappearance of the carboxyl stretching band at 1,700  $\text{cm}^{-1}$ , while carboxylate bands

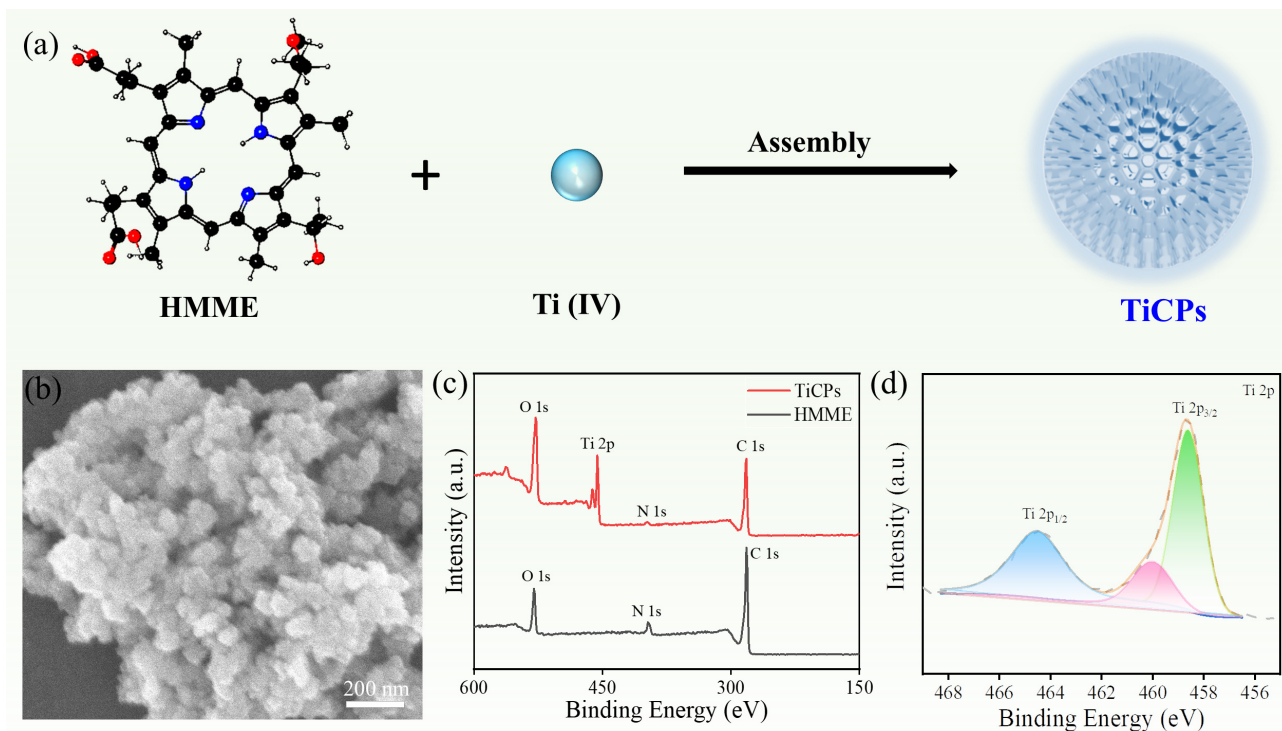


**Figure 1. Synthesis route, morphology and element valence analysis of TiCPs.** (a) Schematic diagram of the preparation of TiCPs; SEM image (b), XPS spectrum (c), and Ti 2p spectrum (d) of TiCPs. HMME: hematoporphyrin monomethyl ether; TiCPs: Ti-HMME coordination nanomaterial

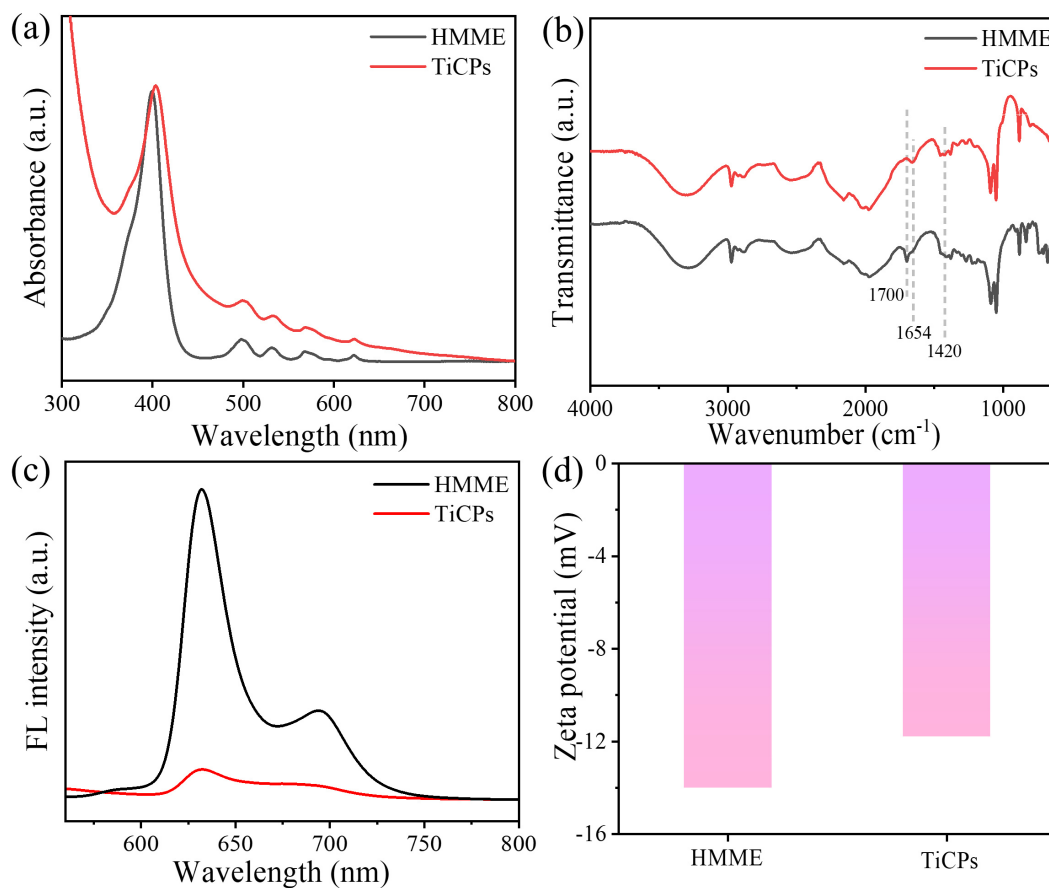


**Figure 2. The interaction between Ti and HMME in TiCPs.** UV-vis absorption spectra (a), Fourier transform infrared (FTIR) spectra (b), fluorescence spectra (c), and zeta potential ( $\zeta$ -potential) (d) of TiCPs and HMME. HMME: hematoporphyrin monomethyl ether; TiCPs: Ti-HMME coordination nanomaterial

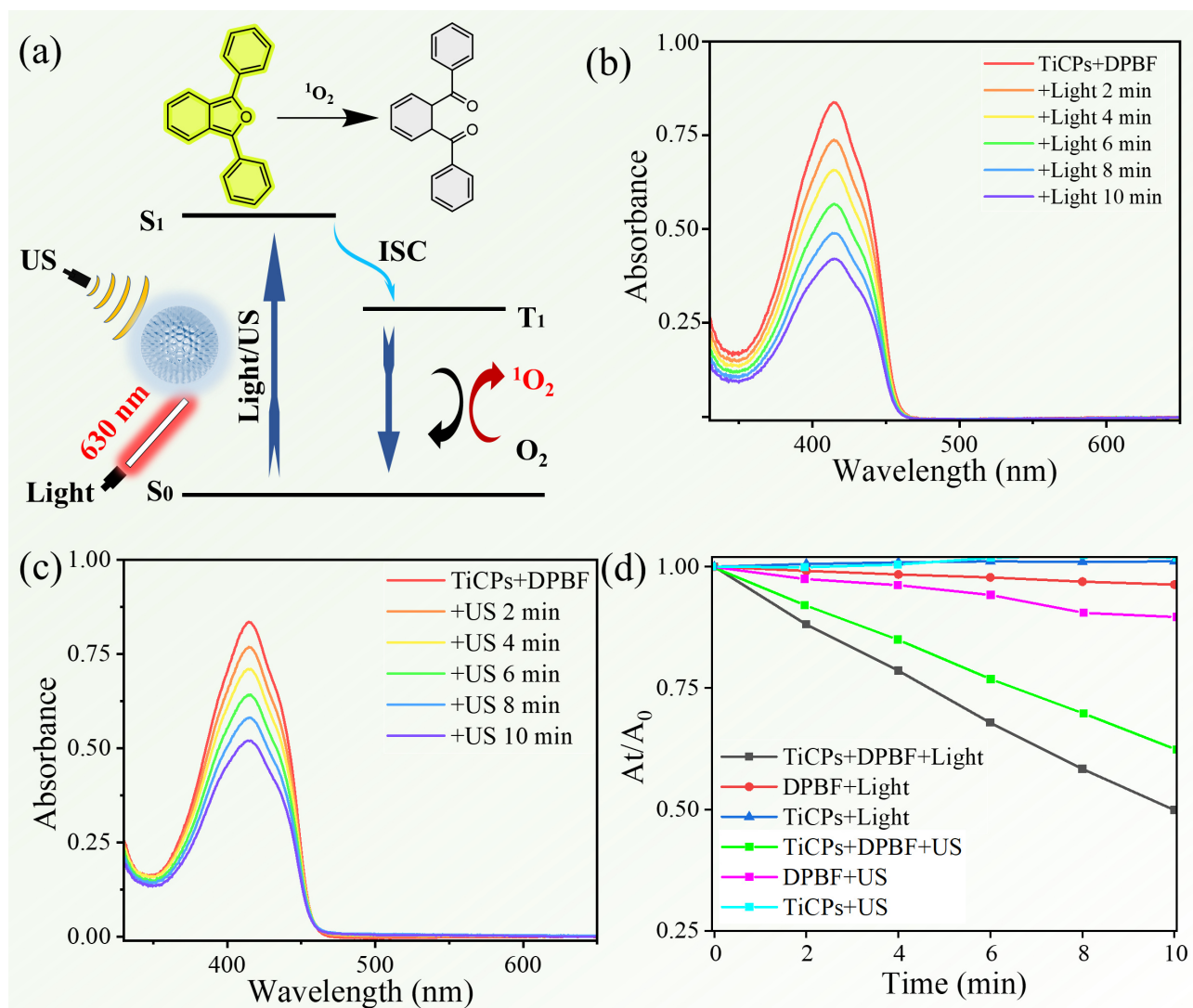


**Figure 3. Evaluate the ability of TiCPs to generate ROS under US/light conditions.** Schematic illustration of ROS generation and DPBF oxidation by TiCPs under light/US excitation (a); absorption spectra of DPBF solution over time under light (b) or US (c) excitation of TiCPs; (d) performance of DPBF under different conditions. TiCPs: Ti-HMME coordination nanomaterial; US: ultrasound

appeared at  $1,654\text{ cm}^{-1}$  and  $1,420\text{ cm}^{-1}$ , indicating successful coordination between  $Ti^{4+}$  ions and the carboxyl groups of HMME (Figure 2b). Additionally, the emission properties of HMME and TiCPs were examined. The free HMME molecule exhibited a strong fluorescence band at 630 nm, whereas the fluorescence of TiCPs was significantly quenched. This quenching is due to  $Ti^{4+}$  ions with unsaturated 3d orbitals, which facilitate energy transfer through low-energy d-d transitions (Figure 2c). Lastly, the Zeta potential analysis indicated a shift from  $-13.9\text{ mV}$  for HMME to  $-11.8\text{ mV}$  for TiCPs, attributed to the positive charge contribution from  $Ti^{4+}$  ions (Figure 2d). Collectively, these results confirm that TiCPs were successfully synthesized through the self-assembly of  $Ti^{4+}$  ions with the carboxyl groups of HMME.

### The ability of TiCPs to generate ROS under US/light conditions

The TiCPs contain the photo/sonosensitizer HMME, which can be activated by light or US to generate ROS [16]. The ROS generation was evaluated using DPBF as the ROS probe (Figure 3a). Upon light irradiation ( $630\text{ nm}$ ,  $100\text{ mW}\cdot\text{cm}^{-2}$ ) of the TiCPs-DPBF mixture, the characteristic absorption peak of DPBF at 415 nm decreased rapidly with increasing irradiation time, indicating effective ROS production by TiCPs under light activation (Figure 3b). Similarly, when the mixture was exposed to US ( $2.0\text{ W}\cdot\text{cm}^{-2}$ , 10 min), the absorbance of DPBF at 415 nm also declined, confirming ROS generation by TiCPs under US activation (Figure 3c).

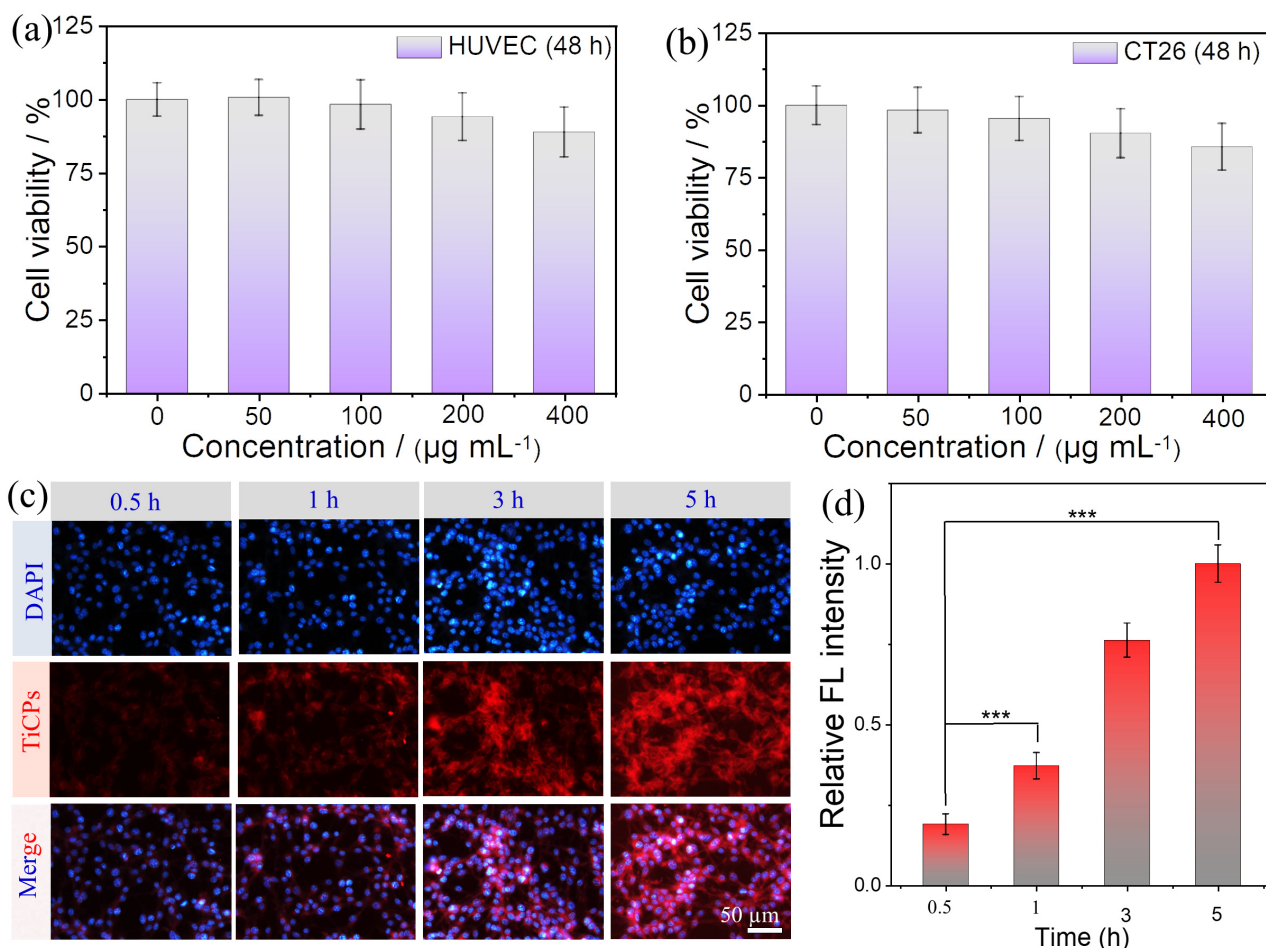


**Figure 4. Evaluate the biocompatibility of TiCPs and their endocytosis/uptake efficiency by CT26 cells.** (a, b) Cell viability of HUVEC and CT26 cells co-cultured with different concentrations of TiCPs for 48 h; Fluorescence images (c) and fluorescence intensity (d) of CT26 cells incubated with TiCPs for different durations. \*\*\* $p < 0.001$ ; TiCPs: Ti-HMME coordination nanomaterial

A summary of ROS generation under various conditions is shown in Figure 3d. After 10 min of light irradiation, the DPBF absorption peak dropped from 0.83 to 0.42, while US exposure for 10 min reduced it from 0.84 to 0.52. These results indicate that 49.4% (light) and 38.1% (US) of the DPBF were oxidized by ROS generated by TiCPs. Control experiments showed minimal changes in absorbance for pure DPBF solution and TiCPs dispersion under light/US treatment (Figures S2 and S3), confirming their stability under these conditions. These findings demonstrate that TiCPs can effectively generate ROS under light and US irradiation, making them promising candidates for subsequent PSDT experiments in tumor cells.

### The biocompatibility of TiCPs and their internalization/uptake efficiency in CT26 cells

To assess the biocompatibility of TiCPs, HUVEC and CT26 were incubated with TiCPs for varying durations, and cell viability was evaluated using the MTT assay. After 24 or 48 h of incubation, both cell lines maintained high viability, with an average survival rate exceeding 85% ( $\leq 400 \mu\text{g}\cdot\text{mL}^{-1}$ ), indicating excellent biocompatibility (Figures 4a and 4b, Figures S4 and S5). TiCPs (200 µg/mL) were cultured in a fresh medium containing CT26 cells and incubated for different time intervals (0.5, 1, 3, and 5 h). After washing with PBS, the cells were stained with DAPI for 30 min. The internalization of TiCPs in CT26 cells was observed using fluorescence imaging under a digital microscope. As shown in Figure 4c, the red fluorescence of TiCPs within the cells gradually increased over time, confirming the effective internalization/uptake of TiCPs. Furthermore, the relative fluorescence intensity of the cells increased as the incubation time extended from 0.5 h to 5 h (compared to 0.5 h, \*\*\* $p < 0.001$ ), indicating a time-dependent uptake of TiCPs by CT26 cells (Figure 4d). These results confirmed that TiCPs have good biocompatibility and can be effectively internalized by CT26 cells.

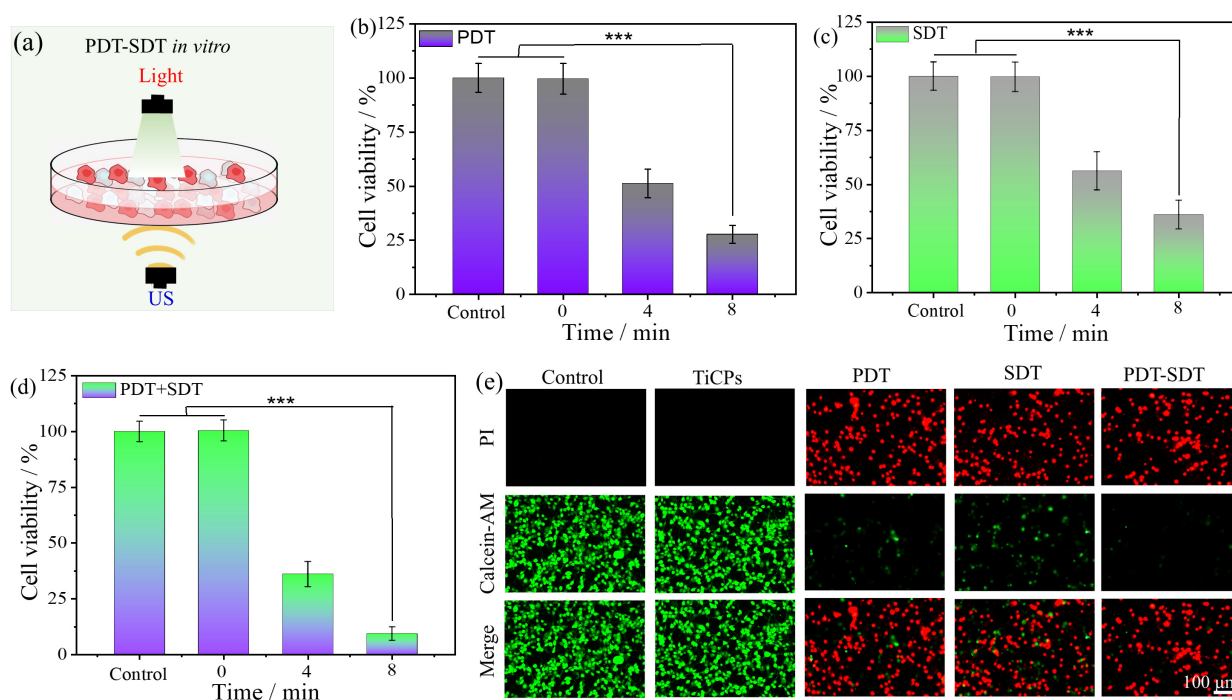


**Figure 5. PSDT therapeutic effect of cells in vitro.** (a) Schematic diagram of PSDT treatment in vitro. (b, c, d) Cell viability under PDT, SDT, and PSDT at different excitation times; (e) Fluorescence images of cells after 8 min of PDT, SDT, and PSDT treatments.  $***p < 0.001$ ; PDT: photodynamic therapy; PSDT: photodynamic-sonodynamic therapy; SDT: sonodynamic therapy; US: ultrasound; TiCPs: Ti-HMME coordination nanomaterial

To investigate the intracellular ROS generation, we used the DCFH-DA staining assay after confirming the internalization of TiCPs. The cells were incubated with a medium containing TiCPs at  $200 \mu\text{g}\cdot\text{mL}^{-1}$  for 4 h, followed by washing with PBS. DCFH-DA ( $20 \mu\text{M}$ ) in serum-free medium ( $100 \mu\text{L}$ ) was then added to the cells. After incubating for 30 min, the cells were exposed to US and/or light and stained with DAPI for 20 min. Finally, cells were washed with PBS and imaged by a digital microscope. For cells in the control group or separately treated with TiCPs, there was no obvious green fluorescence, indicating the absence of ROS within the cells. When cells were treated with TiCPs and 630 nm light ( $100 \text{mW}\cdot\text{cm}^{-2}$ , 5 min), green fluorescence from the oxidized DCFH-DA appeared within cells, which verifies the photodynamic effect of TiCPs. Similarly, green fluorescence was observed when the TiCPs-incubated cells were exposed to US ( $2.0 \text{W}\cdot\text{cm}^{-2}$ , 5 min), confirming the sonodynamic effect of TiCPs within the cells (Figure S6). These results confirm that TiCPs within cells can generate ROS upon light or US exposure, resulting in photodynamic and/or sonodynamic effects.

### PSDT therapeutic effect of cells in vitro

The PDT and SDT effects of TiCPs ( $200 \mu\text{g}\cdot\text{mL}^{-1}$ ) on CT26 tumor cells were subsequently examined in vitro (Figure 5a). For PDT, after co-incubating TiCPs with CT26 cells for 5 h and then exposing them to light ( $630 \text{nm}$ ,  $100 \text{mW}\cdot\text{cm}^{-2}$ ) for 4 or 8 min, cell viability significantly decreased to 51.6% and 28.1% (versus control group,  $***p < 0.001$ ), respectively (Figure 5b). Similarly, in the SDT experiment, cell viability decreased markedly following US ( $2.0 \text{W}\cdot\text{cm}^{-2}$ ) exposure for 4 or 8 min, reaching 56.8% and 36.3% (versus control group,  $***p < 0.001$ ), respectively (Figure 5c). Clearly, extending the duration of light or US exposure enhanced the therapeutic efficacy. Furthermore, the synergistic effects of PSDT were evaluated at different time points (Figure 5d). After co-incubating TiCPs with CT26 cells for 5 h, simultaneous light and US treatment reduced cell viability to 35.6% after 4 min and almost completely eradicated cell viability after 8 min (versus control group,  $***p < 0.001$ ). To visually assess the therapeutic efficacy under different treatment conditions after 8 min, cells were stained with Calcein-AM/PI (Figure 5e). The live/dead cell staining images revealed only partial red fluorescence (dead cells) in the PDT and SDT groups, while the PSDT group exhibited almost exclusively red fluorescence across the field of view, indicating that the combined PSDT treatment effectively killed CT26 cells within 8 min. In summary, these results demonstrate that TiCPs exhibit a highly effective synergistic PSDT therapeutic effect.

## Discussion

In summary, nanoscale TiCPs were successfully synthesized through the self-assembly of  $Ti^{4+}$  ions and HMME using a solvothermal method. Compared to previously utilized multifunctional nanomaterials for PSDT combination therapy, the synthesized “two-in-one” TiCPs offer two distinct advantages: (1) TiCPs are composed of the biocompatible metal element Ti and the clinically approved drug HMME, ensuring excellent biocompatibility; (2) the straightforward self-assembly strategy imparts TiCPs with the ability to generate ROS under light and US excitation conditions, making them suitable for synergistic PSDT in tumor cells. Therefore, this work presents an effective strategy for exploring molecules with structural similarities to HMME for applications in the “all-in-one” multifunctional tumor diagnosis and treatment field.

## Abbreviations

DCFH-DA: 2',7'-dichlorofluorescein diacetate

DPBF: 1,3-Diphenylisobenzofuran

HMME: hematoporphyrin monomethyl ether

MCPs: metal-organic coordination nanomaterials

PDT: photodynamic therapy

PSDT: photodynamic-sonodynamic therapy

PTT: photothermal therapy

ROS: reactive oxygen species

SDT: sonodynamic therapy

SEM: Scanning Electron Microscope

TCPP: tetra (4-carboxyphenyl) porphyrin

TiCPs: Ti-hematoporphyrin monomethyl ether coordination nanomaterial

US: ultrasound

XPS: X-ray Photoelectron Spectrometer

## Supplementary materials

The supplementary figures and other supplementary material for this article are available at: [https://www.explorationpub.com/uploads/Article/file/101337\\_sup\\_1.pdf](https://www.explorationpub.com/uploads/Article/file/101337_sup_1.pdf).

## Declarations

### Author contributions

WW: Investigation, Writing—original draft, Writing—review & editing. YL, WH, LH, HL: Investigation. PG: Conceptualization, Writing—review & editing, Validation, Supervision. SX: Supervision, Funding acquisition, Project administration.

### Conflicts of interest

The authors declare that they have no conflicts of interest.

### Ethical approval

Not applicable.

### Consent to participate

Not applicable.

## Consent to publication

Not applicable.

## Availability of data and materials

Data will be available on reasonable request.

## Funding

This work was supported by the National Natural Science Foundation of China [22171163], the 111 Project [D20015], the Natural Science Foundation of Hubei Province [2024AFB059] and the Yichang Natural Science Research Program [A23-2-025]. The funders had no role in study design, data collection and analysis, decision to publish, or preparation of the manuscript.

## Copyright

© The Author(s) 2025.

## Publisher's note

Open Exploration maintains a neutral stance on jurisdictional claims in published institutional affiliations and maps. All opinions expressed in this article are the personal views of the author(s) and do not represent the stance of the editorial team or the publisher.

## References

1. Sung H, Ferlay J, Siegel RL, Laversanne M, Soerjomataram I, Jemal A, et al. Global Cancer Statistics 2020: GLOBOCAN Estimates of Incidence and Mortality Worldwide for 36 Cancers in 185 Countries. *CA Cancer J Clin.* 2021;71:209–49. [DOI] [PubMed]
2. Siddique A, Garakani MM, Cooke ME, Weber MH, Rosenzweig DH. Nanoparticle-functionalized acrylic bone cement for local therapeutic delivery to spine metastases. *Explor BioMat-X.* 2024;1:135–57. [DOI]
3. Li Y, Wang W, Zhang YT, Xiao SZ, Lan HC, Geng P. Design and Synthesis of Nanoscale Zr-Porphyrin IX Framework for Synergistic Photodynamic and Sonodynamic Therapy of Tumors. *Acta Chim Sinica.* 2024;82:443–8. [DOI]
4. Yang L, Liu Y, Ren X, Jia R, Si L, Bao J, et al. Microemulsion-Assisted Self-Assembly of Indium Porphyrin Photosensitizers with Enhanced Photodynamic Therapy. *ACS Nano.* 2024;18:3161–72. [DOI] [PubMed]
5. Zhang J, Ye W, Wan L, Shi N, Peng C, Shi Y, et al. Beating xenograft liposarcoma using metal selenides with NIR-III photothermal ablation and bioactive selenium derivatives. *Chem Eng J.* 2024;481:148521. [DOI]
6. Geng P, Yu N, Macharia DK, Meng RR, Qiu P, Tao C, et al. MOF-derived CuS@Cu-MOF nanocomposites for synergistic photothermal-chemodynamic-chemo therapy. *Chem Eng J.* 2022;441:135964. [DOI]
7. Li Y, Huang L, Li X, Geng P, Xiang J, Wang W, et al. From biomaterials to biotherapy: cuttlefish ink with protoporphyrin IX nanoconjugates for synergistic sonodynamic-photothermal therapy. *J Mater Chem B.* 2024;12:1837–45. [DOI] [PubMed]
8. Liang S, Xiao X, Bai L, Liu B, Yuan M, Ma P, et al. Conferring Ti-Based MOFs with Defects for Enhanced Sonodynamic Cancer Therapy. *Adv Mater.* 2021;33:e2100333. [DOI] [PubMed]
9. Wang W, Zhang YT, Li Y, Huang YZ, Xiao SZ, Huang WQ, et al. Preparation of cuttlefish ink-porphyrin nanoconjugates and its application in photodynamic-photothermal synergistic treatment of tumor cells. *Nano Med Mater.* 2024;4:1895. [DOI]
10. Geng P, Xiang GC, Zhang W, Lan HC, Xiao SZ. Hollow copper sulfide loaded protoporphyrin for photothermal-sonodynamic therapy of cancer cells. *Chinese J Inorg Chem.* 2024;40:1903–10. [DOI]

11. Gao C, Kwong CHT, Wang Q, Kam H, Xie B, Lee SM, et al. Conjugation of Macrophage-Mimetic Microalgae and Liposome for Antitumor Sonodynamic Immunotherapy via Hypoxia Alleviation and Autophagy Inhibition. *ACS Nano*. 2023;17:4034–49. [DOI] [PubMed]
12. Jia T, Du J, Yang J, Li Y, Ohulchanskyy TY, Fang X, et al. Metalloporphyrin MOFs-Based Nanoagent Enabling Tumor Microenvironment Responsive Sonodynamic Therapy of Intracranial Glioma Signaled by NIR-IIb Luminescence Imaging. *Adv Funct Mater*. 2023;34:2307816. [DOI]
13. Gong F, Cheng L, Yang N, Betzer O, Feng L, Zhou Q, et al. Ultrasmall Oxygen-Deficient Bimetallic Oxide  $MnWO_x$  Nanoparticles for Depletion of Endogenous GSH and Enhanced Sonodynamic Cancer Therapy. *Adv Mater*. 2019;31:e1900730. [DOI] [PubMed]
14. Meng X, Sun S, Gong C, Yang J, Yang Z, Zhang X, et al. Ag-Doped Metal-Organic Frameworks' Heterostructure for Sonodynamic Therapy of Deep-Seated Cancer and Bacterial Infection. *ACS Nano*. 2023;17:1174–86. [DOI] [PubMed]
15. Geng P, Yu N, Liu X, Zhu Q, Wen M, Ren Q, et al. Sub 5 nm  $Gd^{3+}$ -Hemoporphin Framework Nanodots for Augmented Sonodynamic Theranostics and Fast Renal Clearance. *Adv Healthcare Mater*. 2021;10:e2100703. [DOI] [PubMed]
16. Geng P, Li Y, Macharia DK, Ren X, Meng R, Wang W, et al. One Stone, Three Birds: Design and Synthesis of "All-in-One" Nanoscale Mn-Porphyrin Coordination Polymers for Magnetic Resonance Imaging-Guided Synergistic Photodynamic-Sonodynamic Therapy. *J Colloid Interface Sci*. 2024;660:1021–9. [DOI] [PubMed]
17. Liu S, Wen M, Huang M, Wang H, Chen Z, Yu N. Nanoscale hematoporphrin-based frameworks for photo-sono synergistic cancer therapy via utilizing Al(III) as metal nodes rather than heavy metals. *J Colloid Interface Sci*. 2022;616:23–33. [DOI] [PubMed]
18. Zhu J, Wang Y, Yang P, Liu Q, Hu J, Yang W, et al. GPC3-targeted and curcumin-loaded phospholipid microbubbles for sono-photodynamic therapy in liver cancer cells. *Colloids Surf B Biointerfaces*. 2021;197:111358. [DOI] [PubMed]
19. Xu F, Hu M, Liu C, Choi SK. Yolk-structured multifunctional up-conversion nanoparticles for synergistic photodynamic-sonodynamic antibacterial resistance therapy. *Biomater Sci*. 2017;5:678–85. [DOI] [PubMed]
20. Liu Z, Liu S, Liu B, Bian Y, Yuan M, Yang C, et al. Fe(III)-Naphthazarin Metal-Phenolic Networks for Glutathione-Depleting Enhanced Ferroptosis-Apoptosis Combined Cancer Therapy. *Small*. 2023;19:e2207825. [DOI] [PubMed]
21. Xu H, Yu N, Zhang J, Wang Z, Geng P, Wen M, et al. Biocompatible Fe-Hematoporphyrin coordination nanoplatforms with efficient sonodynamic-chemo effects on deep-seated tumors. *Biomaterials*. 2020;257:120239. [DOI] [PubMed]
22. Yu N, Li J, Wang Z, Yang S, Liu Z, Wang Y, et al. Blue Te Nanoneedles with Strong NIR Photothermal and Laser-Enhanced Anticancer Effects as "All-in-One" Nanoagents for Synergistic Thermo-Chemotherapy of Tumors. *Adv Healthcare Mater*. 2018;7:e1800643. [DOI] [PubMed]
23. Zheng Q, Liu X, Zheng Y, Yeung KWK, Cui Z, Liang Y, et al. The recent progress on metal-organic frameworks for phototherapy. *Chem Soc Rev*. 2021;50:5086–125. [DOI] [PubMed]
24. Fan Y, Chen D, Chen L, Liu K, Zheng Y, Li L, et al. Fluorinated Iron Metal-Organic Frameworks for Activatable  $^{19}F$  Magnetic Resonance Imaging and Synergistic Therapy of Tumors. *Nano Lett*. 2023;23:11989–98. [DOI] [PubMed]
25. Geng P, Yu N, Liu X, Wen M, Ren Q, Qiu P, et al. GSH-Sensitive Nanoscale  $Mn^{3+}$ -Sealed Coordination Particles as Activatable Drug Delivery Systems for Synergistic Photodynamic-Chemo Therapy. *ACS Appl Mater Interfaces*. 2021;13:31440–51. [DOI]
26. Geng P, Yu N, Zhang J, Jin Z, Wen M, Jiang Q, et al. One Responsive Stone, Three Birds: Mn(III)-Hemoporphin Frameworks with Glutathione-Enhanced Degradation, MRI, and Sonodynamic Therapy. *Adv Healthcare Mater*. 2021;10:e2001463. [DOI] [PubMed]

27. Zhang K, Meng X, Cao Y, Yang Z, Dong H, Zhang Y, et al. Metal-Organic Framework Nanoshuttle for Synergistic Photodynamic and Low-Temperature Photothermal Therapy. *Adv Funct Mater.* 2018;28:1804634. [DOI]
28. Wang H, Yu D, Fang J, Cao C, Liu Z, Ren J, et al. Renal-Clearable Porphyrinic Metal-Organic Framework Nanodots for Enhanced Photodynamic Therapy. *ACS Nano.* 2019;13:9206–17. [DOI] [PubMed]
29. Kong Q, Qi M, Li W, Shi Y, Su J, Xiao S, et al. A Novel Z-Scheme Heterostructured Bi<sub>2</sub>S<sub>3</sub>/Cu-TCPP Nanocomposite with Synergistically Enhanced Therapeutics against Bacterial Biofilm Infections in Periodontitis. *Small.* 2023;19:e2302547. [DOI] [PubMed]
30. Li B, Wang X, Chen L, Zhou Y, Dang W, Chang J, et al. Ultrathin Cu-TCPP MOF nanosheets: a new theragnostic nanoplatform with magnetic resonance/near-infrared thermal imaging for synergistic phototherapy of cancers. *Theranostics.* 2018;8:4086–96. [DOI] [PubMed] [PMC]
31. Wan S, Cheng Q, Zeng X, Zhang X. A Mn(III)-Sealed Metal-Organic Framework Nanosystem for Redox-Unlocked Tumor Theranostics. *ACS Nano.* 2019;13:6561–71. [DOI] [PubMed]
32. Zhao Y, Kuang Y, Liu M, Wang J, Pei R. Synthesis of Metal–Organic Framework Nanosheets with High Relaxation Rate and Singlet Oxygen Yield. *Chem Mater.* 2018;30:7511–20. [DOI]
33. Wang Z, Liu C, Zhao Y, Hu M, Ma D, Zhang P, et al. Photomagnetic nanoparticles in dual-modality imaging and photo-sonodynamic activity against bacteria. *Chem Eng J.* 2018;356:811–8. [DOI]
34. Zhang H, Chen J, Zhu X, Ren Y, Cao F, Zhu L, et al. Ultrasound induced phase-transition and invisible nanobomb for imaging-guided tumor sonodynamic therapy. *J Mater Chem B.* 2018;6:6108–21. [DOI] [PubMed]
35. Qin Q, Yang M, Shi Y, Cui H, Pan C, Ren W, et al. Mn-doped Ti-based MOFs for magnetic resonance imaging-guided synergistic microwave thermal and microwave dynamic therapy of liver cancer. *Bioact Mater.* 2023;27:72–81. [DOI] [PubMed] [PMC]
36. Xing J, Yang Y, Zhang W, Yan J, Qian H, Hao J, et al. Injectable Hydrogel Containing TiO Nanosheets for Synergistic Photothermal/Thermodynamic Therapy. *ACS Appl Mater Interfaces.* 2023;15:34436–50. [DOI] [PubMed]